Ceramics International 43 (2017) S359–S363

Contents lists available at ScienceDirect

Ceramics International

journal homepage: www.elsevier.com/locate/ceramint

Reassignment of O-related infrared absorption peaks in CdSe

Pimpika Pimsorn[a,b,c], Nirawith Palakawong[a,b,c], Jiraroj T-Thienprasert[c,d,*], Adisak Boonchun[d], Pakpoom Reunchan[d], Sukit Limpijumnong[a,b,c]

[a] School of Physics and NANOTEC-SUT Center of Excellence on Advanced Functional Nanomaterials, Suranaree University of Technology, Nakhon Ratchasima 30000, Thailand
[b] Synchrotron Light Research Institute, Nakhon Ratchasima 30000, Thailand
[c] Thailand Center of Excellence in Physics (ThEP Center), Commission on Higher Education, Bangkok 10400, Thailand
[d] Department of Physics, Faculty of Science, Kasetsart University, Bangkok 10900, Thailand

ARTICLE INFO

Keywords:
First-principles calculations
DFT
Defect
LVM

ABSTRACT

Upon their observation in 2008, the IR absorption peaks at 1094.11, 1107.45, and 1126.33 cm^{-1} of O-doped wurtzite-CdSe sample have been proposed to associate with the local vibrational modes (LVM) of oxygen – vacancy Cd complex defect (O_{Se}-V_{Cd}) (Chen et al., 2008) [8]. Later, first principles calculations by T-Thienprasert et al. reveal that the LVMs of the O_{Se}-V_{Cd} complex defect are actually at 223, 507 and 517 cm^{-1} not in the 1000 cm^{-1} range (T-Thienprasert et al., 2012) [14]; suggesting that the assignment has to be revised. Bastin et al. identified the source of the modes to be a sulfur-oxygen defect complex (Bastin et al., 2014) [11] by intentionally varied the amount of S and analyzed the isotope abundances of S and O from the measurements. In this work, sulfur-oxygen defect complexes in wurtzite-CdSe were studied by first principles calculations. It is found that SO_2 energetically prefers to substitute on the Se site accompanied by a Cd vacancy (V_{Cd}); forming a SO_2-V_{Cd} complex defect. According to the crystal symmetry of CdSe, there are two different V_{Cd} surrounding the Se site that SO_2 occupied. In addition, there are various different orientations of SO_2 relative to the V_{Cd}. The lowest energy configuration is identified. Its local vibrational modes along with the modes of other possible orientations can explain the observed values both in terms of the frequencies and the dipole orientations. Further, our nudged elastic band calculations showed that the rotation barrier of the SO_2 in the complex is quite low; indicating the molecule can rotate at reasonable temperature. This is consistent with the experimental observation that the peaks are broadened and merged into one at high temperatures.

1. Introduction

Electronic and optical properties of materials are significantly affected by the presence of defects or impurities in materials. In case of light impurities (compare to the host atoms), for instance hydrogen, oxygen, nitrogen and sulfur defects, infrared (IR) absorption spectroscopy technique has been shown to be a powerful tool for identifying the local structures of such defects in crystals. When the mass of impurity atoms are significantly lighter than that of the host atoms the local vibrational modes (LVMs) associated with them are clearly separated from the host's crystal phonon. The LVM associated with each defect has unique vibrational frequencies depending on the type and local environments. Therefore, LVMs can serve as a fingerprint for identifying each defect in crystals. However, it is difficult to identify the local structure of defects based solely on experimental LVMs. Independent first-principles calculation is usually needed to aid the identification. A combination of first-principles calculations and IR absorption spectroscopy has been shown to successfully identify the local structure of various defects in crystals, for instance hydrogen-related defects in $SrTiO_3$ [1,2], H- and N-related defects in ZnO [3–5], and O-related defects in CdTe [6,7].

During 2006–2008, G. Chen et al. nicely observed the LVMs of oxygen-related defects in oxygen-doped CdTe and CdSe by using polarized Fourier transform IR (FTIR) absorption spectroscopy [8–10]. For oxygen-doped CdTe samples, at low temperature, they found a low-frequency LVM at 349.79 cm^{-1} accompanied by two higher-frequency LVMs at 1096.78 and 1108.35 cm^{-1} [10]. They found that the two high-frequency modes merge into a broad peak at ~ 1104.49 cm^{-1} when the temperature is increased above ~ 300 K. The low frequency mode was assigned to the LVM of an oxygen substituting for Te atom (O_{Te}), while the two high frequency modes were assigned to the LVMs of a complex defect between O_{Te} and Cd vacancy (O_{Te}-V_{Cd}). For oxygen-doped CdSe samples, at low temperature they again found two strong absorption peaks at γ_1 = 1094.11 and γ_2 =

* Corresponding author at: Department of Physics, Faculty of Science, Kasetsart University, Bangkok 10900, Thailand.
E-mail addresses: pimpika14@gmail.com (P. Pimsorn), fscicwt@ku.ac.th (J. T-Thienprasert), sukit@sut.ac.th (S. Limpijumnong).

http://dx.doi.org/10.1016/j.ceramint.2017.05.231

Available online 26 May 2017

1107.45 cm^{-1} with one additional peak at γ_3 = 1126.33 cm^{-1} [8]. They attributed this additional peak to the lower symmetry of wurtzite structure (CdSe) compared to zincblend structure (CdTe). These three high LVMs also merge into a single broad peak at the temperature above 560 K. They assigned these high-frequency modes to the LVMs of a complex defect between oxygen substituting for Se and Cd vacancy (O_{Se}-V_{Cd}).

Our group recently calculated and confirmed that Chen et al.'s observed value of 348.79 cm^{-1} is indeed consistent with the LVM associated with the O_{Te} in CdTe (the calculated LVM of 338 cm^{-1}) [7]. However, for the O_{Te}-V_{Cd} complex defect, the calculated values are only 467 and 197 cm^{-1} [7], which are quite far from the observed values in the 1000 cm^{-1} region. Similarly, for CdSe, our group calculated the LVM of O_{Se}-V_{Cd} complex defect and obtained the LVMs of 223, 507, and 512 cm^{-1} [7]. Therefore, the observed high-frequency modes in the 1000 cm^{-1} region should come from other O-related defects, not the $O_{Se/Te}$-V_{Cd} complexes.

Recently, Lavrov's group reinvestigated the LVMs of oxygen-related defect in oxygen-doped CdTe and CdSe [11–13]. They found the same LVMs in CdTe and CdSe samples as observed in G. Chen's works [8,10]. However, in their work they intentionally added not only oxygen but also sulfur into both CdTe and CdSe samples. In additional to the modes observed by Chen's group, they also carefully looked and found the corresponding modes that are the results of minority S natural isotopes (^{33}S and ^{34}S). Therefore they claimed that the observed LVMs at ~ 1100 cm^{-1} in CdTe and CdSe samples involve sulfur-oxygen (SO) complex. For CdTe, T-Thienprasert et al. revealed that SO_2 prefers to substitute for Te and binds with a Cd vacancy; forming a SO_2-V_{Cd} complex defect with two possible configurations. The calculated vibrational frequencies are ~ 1094.9 and 1097.4 cm^{-1} in good agreement with the observed values [14]. In addition, SO_2 in such complex defects can rotate from the metastable configuration to the stable configuration at high temperature. This explains the experimental observation that the two frequencies merged into one at high temperature. For CdSe, which has lower crystal symmetry, the SO complex model is more complicated.

One might wonder why unintentionally doped CdSe samples contain sulfur. Se is a rare element that are naturally found in sulfide minerals of copper iron and lead [15]. That is why S is a common impurity in CdSe. Although, both Chen et al. [8–10] and Bastin et al. [11–13] did not report the concentration of defect responsible for the 1100 cm^{-1} modes, low temperature infrared spectroscopy as used by them are known to highly sensitive to even a trace element. The defects with distinctive LVMs with the concentrations as low as 10^{14} cm^{-3} for thick samples (or 10^{18} cm^{-3} for thin films) can be detected [16].

In this work, we employed first-principles calculations to investigate the SO-related defects in CdSe to seek out the energetically stable configurations and their LVMs that fit experimental observed IR absorption peaks in the ~ 1100 cm^{-1} region. To calculate the LVMs, the frozen-phonon approach, which is based on a harmonic approximation, is used. We found that SO_2 in wurtzite-CdSe prefers to bind with V_{Cd} becoming SO_2-V_{Cd} complex defect. There are, however, more possible structures and orientations due to the lower symmetry of wurtzite-CdSe when comparing with the complex in zincblend-CdTe. Their calculated vibrational frequencies are presented and compared with available IR absorption results.

2. Computational method

We used first-principles calculations based on density functional theory (DFT) within local density approximation (LDA) to study sulfur-oxygen related defects in wurtzite-CdSe. The projector augmented wave potentials [17] as implemented in VASP codes [18,19] were employed to describe the electron-ion interactions. The energy cutoff for expanding the plane wave basis set was set at 500 eV and the Monkhorst-Pack scheme [20] with a sampling k-point mesh of 9 × 9 × 9 was used for primitive cell calculations. The calculated lattice parameters of bulk wurtzite-CdSe are a = 4.288 Å and c/a = 1.620, which are in good agreement with the experimental values of a = 4.302 Å and c/a = 1.630 [21]. For defect calculations, we used a so-called supercell approach with a supercell size of 96 atoms. The stability and possibility of defect formation could be investigated by calculating the defect formation energy, which is defined by

$$\Delta H_f(D) = E_{tot}(D^q) - E_{tot}(bulk) + \sum_X n_X \mu_X + q(E_F + E_{VBM} + \Delta V), \quad (1)$$

where $E_{tot}(D^q)$ and $E_{tot}(bulk)$ are the total energy of the supercell containing the defect D in charge state q and that of the supercell without any defect (perfect cell), n_X represents the number of atoms which is added to (removed from, if negative) a supercell to create the defect with the corresponding atomic chemical potential μ_X described below, E_F is the Fermi energy referenced to the valence band maximum (E_{VBM}), and the last term represents the correction term for charged defect [22].

To grow a single crystal wurtzite-CdSe under thermodynamic equilibrium, the following condition must be satisfied

$$E_{tot}(\mathrm{CdSe}) = \mu_{Cd} + \mu_{Se}, \quad (2)$$

where E_{tot}(CdSe) is the total energy per formula unit of CdSe, μ_{Cd} and μ_{Se} are the atomic chemical potentials of Cd and Se, respectively. If μ_{Cd} is limited by the total energy per formula unit of metallic Cd for preventing the existence of such phase in a crystal, we can simply obtain μ_{Se} from Eq. (2). This condition is called Cd-rich growth condition. In opposite, if μ_{Se} is limited by total energy per formula unit of metallic Se, we can again determine μ_{Cd} from Eq. (2). This is called Se-rich growth condition. For the computations of supercell containing S and O, the phase precipitations produced by S and O, such as CdO, $CdSO_4$, CdS, SeO_2, and SO_2, have to be avoided by limiting the chemical potentials of S and O. We found that under Cd-rich growth condition μ_O and μ_S are limited by CdO and CdS phases, respectively. Under Se-rich growth condition, μ_O and μ_S are limited by $CdSO_4$ and SO_2 phases, respectively.

To compare with the observed IR absorption peaks, we calculated the vibrational modes by constructing a full dynamical matrix. The matrix is constructed by calculating the force acting on each atom in each direction (x, y, and z) as it is perturbed to be slightly shifted from its equilibrium position [7]. The eigenvalues and eigenvectors obtained from the dynamical matrix are the vibrational frequencies and vibrational modes, respectively. To test our calculated approach, we calculated the vibrational frequencies of the SO_2 free-molecule and compared with the corresponding experimental values [23] as illustrated in Table 1. The calculated values are in agreement with the experimental values with the errors of less than 4%.

3. Results and discussions

The local structure of bulk wurtzite-CdSe is depicted in Fig. 1(a). In wurtzite structure, each Cd (as well as Se) atom is four-fold coordinated. All three bond distances between Cd and Se atoms lying near the basal plane (perpendicular to the c axis) are equivalent but are slightly differed from that on the c axis. To investigate the SO-related defects in wurtzite-CdSe, we first studied the behavior of isolated S defect by considering two most stable forms, i.e., substitution for Se site (S_{Se}) and interstitial site (S_i). To determine their stability, we calculated the defect formation energies as a function of Fermi-energy under both Cd-rich and Se-rich growth conditions (Fig. 2). We found that S_{Se} and S_i defects are stable in the neutral charge state with the formation energy of S_i substantially higher than that of S_{Se} defect under both Cd-rich and Se-rich growth conditions. This indicates that the majority of S atom is likely to exist in the form of S_{Se} defect as shown in Fig. 1(b). We further studied a SO-defect by introducing an oxygen atom near S_{Se} defect; forming $(SO)_{Se}$ defect. We found that O atom prefers to bind with the S

Table 1
The calculated vibrational frequency associated with a free SO_2 molecule and SO_2-related defects in wurtzite-CdSe in comparison with the experimental measured infrared spectroscopy peaks.

Type	Relative Energy (eV)	Mode[1]	Calculated frequency (cm^{-1})	Observed frequency (cm^{-1})
SO_2 (molecule)		Sym. Anti-Sym. Bending	1122.55 1312.91 499.48	1151.4[2] 1361.8[2] 517.7[2]
SO_2^*		Sym. Anti-Sym.	827.08 937.15	
$[SO_2^*\text{-}V_{Cd}]^a$	0.12	Sym. Anti-Sym.	951.12 1046.09	γ_1 = 1094.11[3]
$[SO_2^*\text{-}V_{Cd}]^{b1}$	0.00	Sym. Anti-Sym.	1007.08 1095.39	γ_2 = 1107.45[3]
$[SO_2^*\text{-}V_{Cd}]^{b2}$	0.00	Sym. Anti-Sym.	1017.99 1103.25	γ_3 = 1126.33[3]
$[SO_2^*\text{-}V_{Cd}]^{b3}$	0.24	Sym. Anti-Sym.	991.04 1122.97	

[1] Sym = Symmetric stretching mode; Anti-Sym. = Anti-Symmetric stretching mode.
[2] Ref. [8,23].
[3] Ref. [8,23].

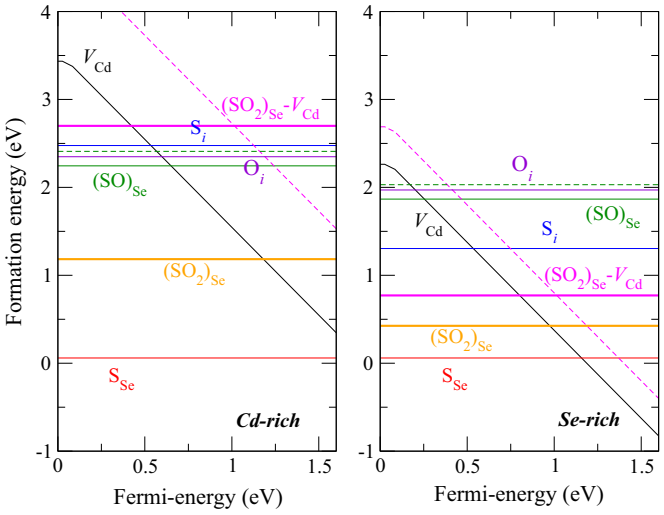

Fig. 2. Defect formation energies as a function of Fermi energy under Cd-rich (left panel) and Se-rich (right-panel) growth conditions. The slope of each line indicates the charge of each defect. The Fermi-energy is plotted from the valence band maximum of CdSe up to the calculated band gap at the special *k*-point to reduce the well-known DFT band gap underestimation.

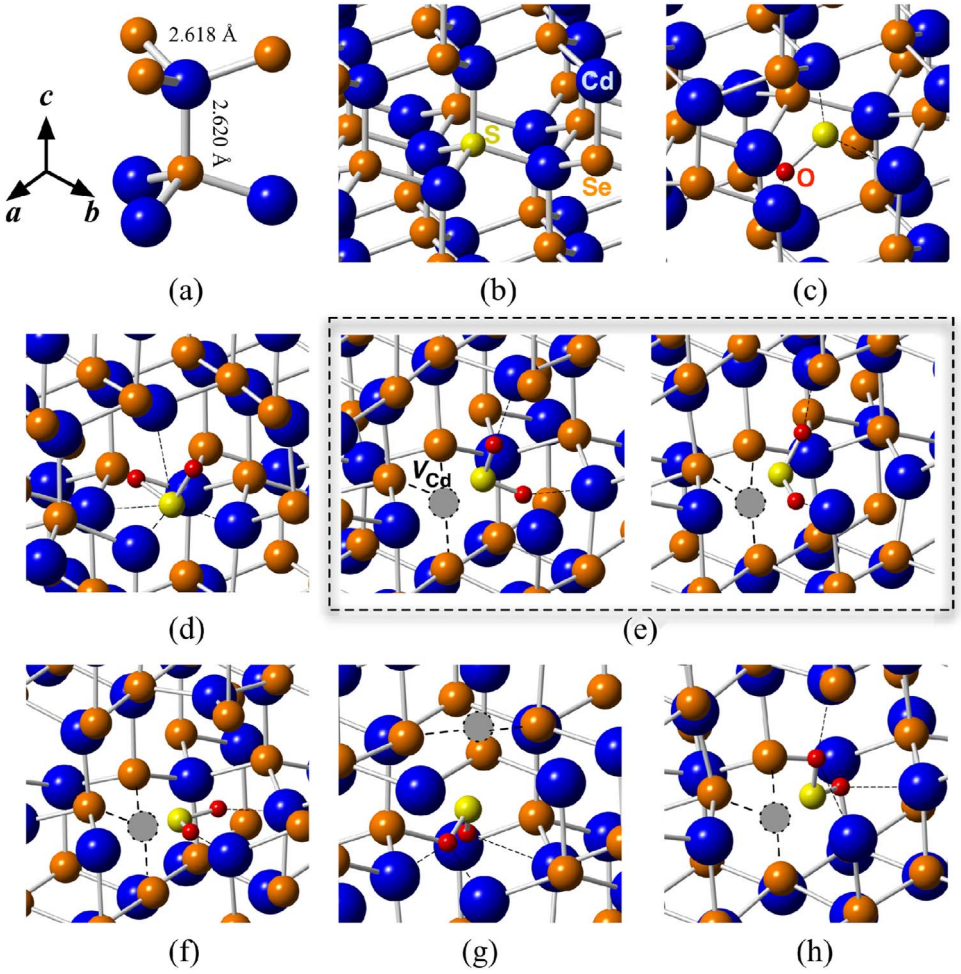

Fig. 1. Schematic illustration of (a) bulk CdSe, (b) S_{Se}, (c) $(SO)_{Se}$, (d) SO_2^*, (e) $[SO_2^*\text{-}V_{Cd}]^{b1}$, (f) $[SO_2^*\text{-}V_{Cd}]^{b2}$, (g) $[SO_2^*\text{-}V_{Cd}]^a$ and (h) $[SO_2^*\text{-}V_{Cd}]^{b3}$. The blue, blown, red, and yellow spheres represent Cd, Se, O, and S atoms, respectively. (For interpretation of the references to color in this figure legend, the reader is referred to the web version of this article.).

atom forming a dumbbell-like structure as shown in Fig. 1(c). The calculation shows that $(SO)_{Se}$ is also stable in the neutral charge state. However, the formation energy of $(SO)_{Se}$ is quite high under both Cd-rich and Se-rich growth conditions. The binding energy of $(SO)_{Se}$ is calculated based on the difference between the sum of the formation energy of isolated defects ($\Delta H_f(S_{Se}) + \Delta H_f(O_i)$ defects) and the formation energy of $(SO)_{Se}$. In Fig. 2, the two energies are shown using dashed and filled green lines, respectively. Note that O_i defect is charge neutral. Both S and O prefer to form bonds with host Cd atoms and share the Se site. The binding energy of $(SO)_{Se}$ is only ~0.16 eV, which is quite low; indicating that $(SO)_{Se}$ could form in a low concentration. If another oxygen is added to $(SO)_{Se}$, the SO_2^* defect can be formed as shown in Fig. 1(d). Note that, the star symbol '*' is used to distinguish it from the SO_2 free-molecule. This SO_2^* is also charge neutral and it looks similar to SO_2 free-molecule. Interestingly, the formation energy of SO_2^* defect is quite low, especially under Se-rich growth condition. The binding energy of SO_2^* defect is 3.41 eV, which is very high. This indicates that S atom prefers to bond with two oxygen atoms to form SO_2^*.

We directly calculated the vibrational modes of SO_2^*. The calculated vibrational frequencies of SO_2^* are 827 and 937 cm^{-1} for the symmetric and anti-symmetric stretching modes, respectively. (Note that the observed IR peaks should relate to anti-symmetric stretching modes. The symmetric stretching mode has a very weak oscillator strength for infrared spectroscopy.) These calculated values are significantly lower than the observed IR peaks at ~ 1100 cm^{-1}. This suggests that SO_2^* is not the origin of the observed peaks at ~ 1100 cm^{-1} in CdSe sample. We further investigated complex defects between SO_2^* and other dominant native defects to seek out the source of the 1100 cm^{-1} mode. Vacancy defects are generally abundant native defects in most materials. In this case, we found that a Cd next to SO_2^* can be removed; forming SO_2^*-V_{Cd} complex defects. Removing a Cd atom helps relief the strain near SO_2^*, which could effectively increase the vibrational frequencies of SO_2^*. As shown in Fig. 1(d), there are two distinct Cd atoms which could be removed to create the SO_2^*-V_{Cd} complex defects, i.e., beside or above SO_2^* defect as shown in Fig. 1(e) – (g). In addition, there are many possible orientations of SO_2^* in each complex structure. In Fig. 1(e) and (f), we illustrate the most stable structures of SO_2^*-V_{Cd} complexes for two nonequivalent configurations that we named them $[SO_2^*\text{-}V_{Cd}]^{b1}$ and $[SO_2^*\text{-}V_{Cd}]^{b2}$, respectively, where the superscript "b" stands for "beside". The energies of $[SO_2^*\text{-}V_{Cd}]^{b1}$ and $[SO_2^*\text{-}V_{Cd}]^{b2}$ are almost identical; indicating that they can co-exist in a comparable concentration. Note that there are two equivalent configurations for $[SO_2^*\text{-}V_{Cd}]^{b1}$ as shown in Fig. 1(e). In Fig. 1(g), we show the structure of SO_2^*-V_{Cd} complex when V_{Cd} is created above SO_2^* defect. This complex is named as $[SO_2^*\text{-}V_{Cd}]^{a}$, where the superscript "a" stands for "above". The calculated relative energies for different SO_2^*-V_{Cd} complexes are shown in Table 1. The formation energy of $[SO_2^*\text{-}V_{Cd}]^{b1/b2}$ is lower than $[SO_2^*\text{-}V_{Cd}]^{a}$; indicating that the former is more likely to form in CdSe sample. The $[SO_2^*\text{-}V_{Cd}]^{b1/b2}$ complexes are stable in the neutral charge state and have low formation energies, especially under the Se-rich growth condition. In order to determine the stability, we calculated the binding energy of the complex. In Fig. 2, the dashed pink line represents the sum of the formation energies of the parent isolated defects, i.e., $\Delta H_f(SO_2^*) + \Delta H_f(V_{Cd})$. The binding energy between the SO_2^* and V_{Cd} to form $[SO_2\text{-}V_{Cd}]^{b1/b2}$ complex is the energy difference between the dashed and filled pink lines. The binding energy is high when the Fermi energy is in the bottom region of CdSe band gap (i.e., ~ 1 eV from the VBM). However, when the Fermi level is close to the conduction band edge the complex is unbound. In the crystal growth process [8], the CdSe sample was grown with the addition of SeO to provide oxygen and excess Se to suppress the formation of Se vacancy. In other words, the CdSe sample was grown under Se-rich condition. Under Se-rich condition, V_{Cd} defect, which is an acceptor, has low formation energy and becomes a major native defect. Therefore, the Fermi level of SO-doped CdSe sample should be near the VBM; implying that SO_2^*-V_{Cd} complex defects could exist in the sample.

The vibrational frequencies associated with the SO_2^*-V_{Cd} complexes are calculated and compared with the observed values in Table 1. The vibrational frequencies of the anti-symmetric stretching vibrational modes associated with $[SO_2^*\text{-}V_{Cd}]^{b1}$ and $[SO_2^*\text{-}V_{Cd}]^{b2}$ complexes are 1095.39 and 1103.25 cm^{-1}, respectively. These are close to the most dominant observed peaks γ_1 = 1094.11 and γ_2 = 1107.45 cm^{-1}. The $[SO_2^*\text{-}V_{Cd}]^{a}$ complex gives a somewhat lower frequency than the observed values. As explained earlier, the symmetric stretch modes have small oscillator strengths and are unlikely to be observed in infrared spectroscopy measurement. Therefore, the observed vibrational frequencies γ_1 and γ_2 modes should belong to the vibrational modes of $[SO_2^*\text{-}V_{Cd}]^{b1}$ and $[SO_2^*\text{-}V_{Cd}]^{b2}$ complexes, respectively. The fact that the formation energy of $[SO_2^*\text{-}V_{Cd}]^{a}$ is higher than that of $[SO_2^*\text{-}V_{Cd}]^{b1/b2}$ also support this assignment. In experiment, by using polarized IR absorption measurement, the vibrational direction of γ_1, γ_2, and γ_3 modes are determined. It is found that the oscillator direction of γ_2 mode lies close to the basal plane (almost perpendicular to the $\hat{\mathbf{c}}$ axis). On the other hand, the oscillator directions of γ_1 and γ_3 modes are pointing by a significant angle (> 45°) away from the basal plane. From our calculated results, the vibrational direction of S-O in $[SO_2\text{-}V_{Cd}]^{b2}$ (see Fig. 1(f)) is almost perpendicular to $\hat{\mathbf{c}}$ axis, while that of S-O in $[SO_2\text{-}V_{Cd}]^{b1}$ (see Fig. 1e) make some angle with respect to $\hat{\mathbf{c}}$ axis. Therefore, the calculated formation energies, vibrational frequencies and structures are all consistent to assign γ_1 and γ_2 modes to $[SO_2^*\text{-}V_{Cd}]^{b1}$ and $[SO_2^*\text{-}V_{Cd}]^{b2}$ complexes, respectively. However, the observed vibrational frequency γ_3 at 1126.33 cm^{-1}, which is a minority peak, is left unexplained.

We further explored other meta-stable structures by rotating SO_2^* in both $[SO_2\text{-}V_{Cd}]^{b1}$ and $[SO_2\text{-}V_{Cd}]^{b2}$ complexes. If the SO_2^* in $[SO_2\text{-}V_{Cd}]^{b1}$ is rotated away from the equilibrium position and it can be trapped in a metastable state as shown in Fig. 1(h). We will call this state $[SO_2\text{-}V_{Cd}]^{b3}$ complex. The total energy of this metastable state is 0.24 eV higher than the ground state $[SO_2\text{-}V_{Cd}]^{b1}$ complex. Therefore, it should exist in a low concentration compared to the ground state one. The calculated vibrational frequencies of $[SO_2\text{-}V_{Cd}]^{b3}$ are also tabulated in Table 1. The calculated anti-symmetric stretching vibrational frequency is in good agreement with the γ_3 mode. The $[SO_2\text{-}V_{Cd}]^{b3}$ complex is related with $[SO_2\text{-}V_{Cd}]^{b1}$ by a simple rotation of SO_2^* and the orientation of SO_2^* in these two complexes are quite similar [Fig. 1(e) and (h)].

The $[SO_2\text{-}V_{Cd}]^{b1}$, $[SO_2\text{-}V_{Cd}]^{b2}$, and $[SO_2\text{-}V_{Cd}]^{b3}$ complexes are related to each other by a simple rotation of the SO_2^*. We have determined the rotational barriers separating each local minima by using a climbing nudge elastic band method [24–27] (cNEB) as implemented in VASP code. Fig. 3 shows the calculated relative energy as a function of configuration coordinate, where the total energy is

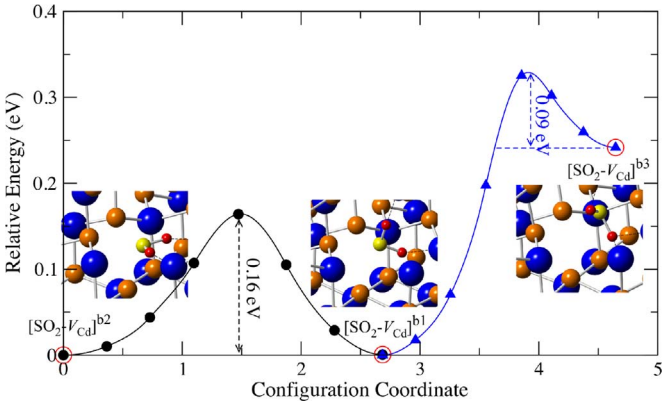

Fig. 3. Calculated energy of the SO_2^*-V_{Cd} complex as SO_2^* in the complex is rotate to form three different configurations. The total energy on the $\hat{\mathbf{y}}$ axis is referenced to that of the $[SO_2\text{-}V_{Cd}]^{b1}$ complex.

referenced to that of $[SO_2\text{-}V_{Cd}]^{b1}$ complex. Based on our calculated results, we found that the migration barrier for rotating SO_2^* between $[SO_2\text{-}V_{Cd}]^{b1}$ and $[SO_2\text{-}V_{Cd}]^{b2}$ complexes and that between $[SO_2\text{-}V_{Cd}]^{b1}$ and $[SO_2\text{-}V_{Cd}]^{b3}$ complexes are only 0.16 and 0.09 eV, respectively. These low migration barriers indicate that SO_2^* could rotate and populate the three structures at reasonably low temperatures. At a reasonably high temperature the meta-sable configuration $[SO_2\text{-}V_{Cd}]^{b3}$ can also be populated and the configuration is trapped after cooled down; resulting in a minority peak γ_3. The experiment results also showed that the three sharp peaks at ~ 1100 cm^{-1} at very low temperature of 5 K are broadened and merged into one when increasing the temperature [8,9]. This is consistent with the rather low rotation barriers we calculated. Based on our calculated results, the γ_1, γ_2, and γ_3 modes are consistent with the vibrational modes of $[SO_2\text{-}V_{Cd}]^{b1}$, $[SO_2\text{-}V_{Cd}]^{b2}$, and $[SO_2\text{-}V_{Cd}]^{b3}$, respectively.

4. Conclusion

Using first-principles DFT calculations, we investigated the origin of the observed IR absorption peaks at γ_1 = 1094.11, γ_2 = 1107.45 cm^{-1}, and γ_3 = 1126.33 cm^{-1}, which are proposed to be related to the SO_2 complex defects in wurtzite-CdSe. We found that SO_2 prefers to substitute on the Se-site accompanied by a Cd vacancy; forming a $SO_2\text{-}V_{Cd}$ complex. The SO_2^* in such complex can rotate and trapped in two stable configurations with almost exactly the same energy with a meta-stable structure that are named $[SO_2\text{-}V_{Cd}]^{b1}$, $[SO_2\text{-}V_{Cd}]^{b2}$ and $[SO_2\text{-}V_{Cd}]^{b3}$, respectively. Our calculated vibrational frequencies associated with the three complexes are in good agreement with the observed values of the γ_1, γ_2, and γ_3 modes. By using cNEB method, we found that the migration barriers for rotating SO_2^* are quite low; indicating that SO_2^* can easily rotate. This could make the observed peaks broadening and merged into one as the temperature increased.

Conflict of interest

We declare that we do not have any commercial or associative interest that represents a conflict of interest in connection with the work submitted.

Acknowledgments

This work was partially supported by NANOTEC, NSTDA (Thailand) through its Center of Excellence Network program. P.P. acknowledges the support from the OROG scholarship through Suranaree University of Technology and the Thailand Center of Excellence in Physics (ThEP Center), Commission on Higher Education, Bangkok, Thailand. J.T. is supported by Kasetsart University Research and Development Institute (KURDI).

References

[1] I. Fongkaew, J. T-Thienprasert, D.J. Singh, M.H. Du, S. Limpijumnong, First principles calculations of Hydrogen-Titanium vacancy complexes in $SrTiO_3$, Ceram. Int. 39 (2013) S273.
[2] J. T-Thienprasert, I. Fongkaew, D.J. Singh, M.H. Du, S. Limpijumnong, Identification of hydrogen defects in $SrTiO_3$ by first-principles local vibration mode calculations, Phys. Rev. B 85 (2012) 125205.
[3] S. Limpijumnong, X.N. Li, S.H. Wei, S.B. Zhang, Probing deactivations in Nitrogen doped ZnO by vibrational signatures: a first principles study, Physica B 376 (2006) 686.
[4] S. Limpijumnong, S.B. Zhang, Resolving hydrogen binding sites by pressure – a first-principles prediction for ZnO, Appl. Phys. Lett. 86 (2005) 151910.
[5] X. Li, B. Keyes, S. Asher, S.B. Zhang, S.-H. Wei, T.J. Coutts, S. Limpijumnong, C.G. Van de Walle, Hydrogen passivation effect in nitrogen-doped ZnO thin films, Appl. Phys. Lett. 86 (2005) 122107.
[6] J. T-Thienprasert, T. Watcharatharapong, I. Fongkaew, M.H. Du, D.J. Singh, S. Limpijumnong, Identification of oxygen defects in CdTe revisited: first-principles study, J. Appl. Phys. 115 (2014) 203511.
[7] J. T-Thienprasert, S. Limpijumnong, A. Janotti, C.G. Van de Walle, L. Zhang, M.H. Du, D.J. Singh, Vibrational signatures of O_{Te} and O_{Te}-V_{Cd} in CdTe: a first-principles study, Comput. Mater. Sci. 49 (2010) S242.
[8] G. Chen, J.S. Bhosale, I. Miotkowski, A.K. Ramdas, Spectroscopic signatures of novel oxygen-defect complexes in stoichiometrically controlled CdSe, Phys. Rev. Lett. 101 (2008) 195502.
[9] G. Chen, I. Miotkowski, S. Rodriguez, A.K. Ramdas, Control of defect structure in compound semiconductors with stoichiometry: oxygen in CdTe, Phys. Rev. B 75 (2007) 125204.
[10] G. Chen, I. Miotkowski, S. Rodriguez, A.K. Ramdas, Stoichiometry driven impurity configurations in compound semiconductors, Phys. Rev. Lett. 96 (2006) 035508.
[11] D. Bastin, E.V. Lavrov, J. Weber, Reassignment of the O_{Se}–V_{Cd} complex in CdSe, AIP Conf. Proc. 1583 (2014) 169.
[12] D. Bastin, E.V. Lavrov, J. Weber, Cadmium vacancy passivated by two hydrogen atoms in CdSe, Phys. Rev. B 85 (2012) 195204.
[13] E.V. Lavrov, D. Bastin, J. Weber, J. Schneider, A. Fauler, M. Fiederle, Reassignment of the O_{Te}-V_{Cd} complex in CdTe, Phys. Rev. B 84 (2011) 233201.
[14] J. T-Thienprasert, S. Limpijumnong, M.H. Du, D.J. Singh, First principles study of O defects in CdSe, Physica B 407 (2012) 2841.
[15] Sources of selenium and tellurium, ⟨http://www.stda.org/se_te.html⟩, 2017.
[16] M. Stavola, Identification of defects in semiconductors, Academic Press, United States Of America, 1999.
[17] G. Kresse, D. Joubert, From ultrasoft pseudopotentials to the projector augmented-wave method, Phys. Rev. B 59 (1999) 1758.
[18] G. Kresse, J. Furthmüller, Efficiency of ab-initio total energy calculations for metals and semiconductors using a plane-wave basis set, Comput. Mater. Sci. 6 (1996) 15.
[19] G. Kresse, J. Hafner, Norm-conserving and ultrasoft pseudopotentials for first-row and transition-elements, J. Phys. Condens. Matter 6 (1994) 8245.
[20] H.J. Monkhorst, J.D. Pack, Special points for Brillouin-zone integrations, Phys. Rev. B 13 (1976) 5188.
[21] U. Hotje, C. Rose, M. Binnewies, Lattice constants and molar volume in the system ZnS, ZnSe, CdS, CdSe, Solid State Sci. 5 (2003) 1259.
[22] C.G. Van de Walle, J. Neugebauer, First-principles calculations for defects and impurities: applications to III-nitrides, J. Appl. Phys. 95 (2004) 3851.
[23] W.B. Person, G. Zerbi, Vibrational Intensities in Infrared and Raman Spectroscopy, Elsevier, Amsterdam, 1982.
[24] D. Sheppard, R. Terrell, G. Henkelman, Optimization methods for finding minimum energy paths, J. Chem. Phys. 128 (2008) 134106.
[25] G. Henkelman, B.P. Uberuaga, H. Jónsson, A climbing image nudged elastic band method for finding saddle points and minimum energy paths, J. Chem. Phys. 113 (2000) 9901.
[26] G. Henkelman, H. Jónsson, Improved tangent estimate in the nudged elastic band method for finding minimum energy paths and saddle points, J. Chem. Phys. 113 (2000) 9978.
[27] G. Mills, H. Jónsson, G.K. Schenter, Reversible work transition state theory: application to dissociative adsorption of hydrogen, Surf. Sci. 324 (1995) 305.